AIChE

Magnetic Resonance Imaging Study of Complex Flow of Viscoelastic Fluids

Giuseppe Maddinelli
Eni S.p.A., R&M Div, via F. Maritano 26, 20097, S. Donato M., Milan, Italy

Alberto Guarneri
Eni S.p.A., E&P Div, via dell'Unione Europea 6, 20097 S. Donato M., Milan, Italy

Stefano Carminati
Eni S.p.A., E&P Div, via dell'Unione Europea 3, 20097, S. Donato M., Milan, Italy

DOI 10.1002/aic.12354
Published online August 16, 2010 in Wiley Online Library (wileyonlinelibrary.com).

NMR imaging techniques have been applied to investigate complex fluid dynamics in pipes and in annular flow conditions. In this application, aimed to simulate drilling and production operations, two lines have been set up to reproduce, at small laboratory scale, respectively, a pipe flow and an annular flow that are typical flow geometries in oilfield wells during drilling. NMR imaging measurements have been performed inside a horizontal-bore magnet with a fluid flow assured in a velocity range of 10–100 cm s^{-1}. The studies were dedicated to investigate the different flow regimes associated to circulating viscous polymer solutions applied in drilling mud formulations. Early transitions from laminar to turbulent regime were observed at very low Reynolds number (in a range between 300 and 500, to be compared with the theoretical transition value greater than 2100). © 2010 American Institute of Chemical Engineers
AIChE J, 57: 1393–1401, 2011
Keywords: NMR imaging, MRI, flow, polymers, turbulence

Introduction

The understanding of complex fluids flow behavior is a key factor to optimize processes in many industrial applications. Nuclear magnetic resonance imaging (MRI) has proven to be particularly useful for studying complex engineering processes,[1] mainly for its noninvasive feature and its high sensitivity to fluid mobility properties. From this point of view, the most promising applications are based on the velocity measurements methods, which rely on the combination of pulsed field gradient spin-echo (PGSE) and imaging experiments.[2] This type of technique has been widely applied in the recent years to investigate transport processes. Applications ranged from monitoring velocity profiles of fluids flowing in simple geometries to identify laminar and turbulent regimes, to the characterization of flow in complex systems (e.g., reactor vessels, porous artificial materials or natural rocks).[1,3] Focusing on the oil industry, fluid transport is present in most of the activities: from exploration, where engineered fluids are used in drilling wells to reach hydrocarbon reservoirs in the subterranean geological structures, to hydrocarbon transportation via pipeline and from the reservoir to a refinery for final processing and transformations. In drilling operations, to sustain the borehole walls, transporting the small cuttings of drilled rock from the hole to the surface and operate in safe conditions, engineered fluids must be properly formulated. Fluid rheological properties in the due temperature interval (up to 220°C) and flow regimes (generally laminar in the upper and larger well sections and turbulent in the deepest and smallest ones) must be guaranteed and maintained. Particularly critical is to maintain good hole cleaning, removing drilled solids (cuttings), while

Correspondence concerning this article should be addressed to G. Maddinelli at giuseppe.maddinelli@eni.com.

keeping pressure losses at minimum, with drilling fluids that can even double the water density. Such a delicate matter is the topic of this work, aimed to clarify the fluid-flow macroscopic and microscopic behavior in pipes and typical wellbore geometries during drilling for representative fluid-flow regimes and under different regimes. Our investigation, performed with imaging techniques, allows direct measurement of dynamic parameters and can provide a simulation testing at laboratory scale useful to validate the numerical modeling of the occurring processes.

MRI methods

The MRI experiments were realized on a Varian NMR spectrometer, constituted by an Oxford 2-T horizontal superconducting magnet, operating at a proton resonance frequency of 85 MHz, equipped with highly shielded gradient coils with a gradient strength up to 7 G cm^{-1} in all the three spatial directions. All NMR experiments were conducted at room temperature, using a 4-cm-diameter Litz-type radiofrequency (RF) coil. For an introduction of the basic principles of MRI experiments, the reader is referred elsewhere.[2]

Velocity measurement methods

A gradient echo-based sequence with two additional flow-encoding pulsed magnetic field gradients was applied and the basic pulse scheme is reported in Figure 1a. The velocity measurements were realized by applying the classical approach based on a phase-shift encoding method.[3] These kinds of experiments are performed with two spatial and one velocity dimensions. The velocity information is encoded for each voxel of the two spatial dimensions by applying a couple of bipolar gradients. These flow-encoding gradients ($\mathbf{g}_{flow}$), characterized by a duration time δ, induce a phase shift over the time scale Δ. The magnetization phase shift ϕ due to the displacement of the spins is:

$$\phi = \gamma \mathbf{V} \int \mathbf{G}_v(t) t dt \tag{1}$$

where $\mathbf{V}$ is the average velocity of the fluid in the voxel, t is time, γ is the gyromagnetic ratio, $\mathbf{G}_v(t)$ is the time-dependent magnetic field gradient to encode velocity information. For example, considering the movement along the z-direction, the time average of each spin's velocity is defined as:

$$\mathbf{V} = \mathbf{Z}/\Delta \tag{2}$$

where $\mathbf{Z} = \mathbf{z}(\Delta) - \mathbf{z}(0)$ is the displacement in the z-direction, during Δ time. Stationary spins will accumulate a phase shift during the positive gradient that will be cancelled by the negative-going gradient. However, the flowing spins will accumulate a net phase shift that is related to their constant velocity that is obtained by the integration of Eq. 1, which will yield to:

$$\phi = 2\gamma \boldsymbol{V} g(\delta)^2 \tag{3}$$

where g is the magnitude of the intensity of the flow gradients applied. In our application, following a 90° pulse, a duration δ of 1 ms, a maximum gradient intensity of 2 G cm^{-1}, an echo time TE = 0.012 s, a recovery time TR = 0.5 s, and 128 phase-encoding increments were typically used. The imaginary and real images (256 × 256 pixels) were than computed to extract phase-shift information to be related to spin velocity.[4,5]

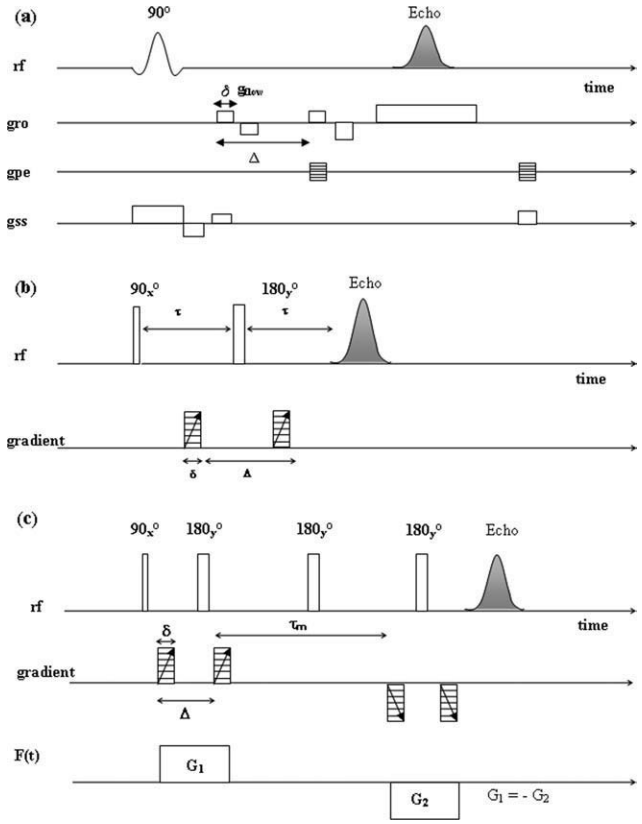

Figure 1. Pulse scheme of the MRI sequences.

(a) gradient echo sequence, with the flow encoding (g_{flow}), read-out gradient (gro), phase encoding (gpe) and slice selective (gss) gradients used to image the velocity field in the 2D image slice; (b) pulsed field gradients spin echo sequence; (c) one dimensional-double PGSE NMR compensated encoding sequence in which the values of the two gradient pulse pairs (G_1 and G_2) are stepped together. For each pair, the effective gradient time integral, F(t), is shown.

PGSE experiments

In the case of the investigation on flow dispersion related to incoherent phenomena, more appropriate techniques based on PGSE NMR experiments[2] could be applied. The basic PGSE NMR pulse sequence, is shown in Figure 1b, and is based on a main RF spin-echo sequence, combined with a pair of narrow magnetic-field gradient pulses (with $\delta << \Delta$, which phase encode the NMR signal for translational displacements over a fixed time interval (Δ). If P_s ($\mathbf{Z}$, Δ) is the average probability, or propagator, for a spin to have a translation $\mathbf{Z}$ from $\mathbf{z}$ to $\mathbf{z}'$, where $\mathbf{Z} = \mathbf{z}' - \mathbf{z}$, during the time Δ, the attenuation function $E(\mathbf{q})$ can be written as

$$E(\mathbf{q}) = \int P_s(\mathbf{Z}, \Delta) \exp(i2\pi \mathbf{q} \cdot \mathbf{Z}) d\mathbf{Z} \tag{4}$$

where the wave vector $\mathbf{q} = (2\pi)^{-1}\gamma \mathbf{g}\delta$ is related to the effect of the two-stepped gradients. The propagator $P_s(\mathbf{Z}, \Delta)$ is obtained from the signal intensity by Fourier transformation with respect to $\mathbf{q}$.

The use of an additional pair of bipolar gradients[4,6–8] leads to an NMR sequence known as double PGSE NMR experiment (Figure 1c), which results in a phase shift useful to compare two displacements or velocities over an evolution (or exchange) time τ_m. In the case of a compensated double PGSE sequence,[6–8] the two pulse pairs have their $\mathbf{q}$ values linked. Considering $\mathbf{q_1}$ (first pair) and $\mathbf{q_2}$ (second pair), where $\mathbf{q_1} = -\mathbf{q_2} = \mathbf{q}$, a one-dimensional data acquisition results. Let the displacements in the first and second encoding pairs be $\mathbf{Z_1} = \mathbf{z}' - \mathbf{z}$ and $\mathbf{Z_2} = \mathbf{z}''' - \mathbf{z}''$, provided that Δ and of course δ, will be sufficiently short to consider a steady-state velocity $\mathbf{v_1} = \mathbf{Z_1}/\Delta$, during the period Δ and analogously a $\mathbf{v_2} = \mathbf{Z_2}/\Delta$, at the second pair. The echo amplitude is given by:

$$E(\mathbf{q}) = \int P_s(\mathbf{V}, \Delta) \exp(i2\pi\mathbf{q} \cdot \mathbf{V}\Delta) d\mathbf{V} \tag{5}$$

where $P_s(\mathbf{V}, \Delta)$ is the average probability, also called average propagator, for velocity variations $\mathbf{V} = \mathbf{v_2} - \mathbf{v_1}$. The effect of applying an additional pair of opposing pulsed field gradients is then to give a net phase shift, which will encode the spins for their change in average velocity over time Δ, after an evolution period of time τ_m, between the pulse pairs. This NMR method is useful in evaluating the presence of fluctuations or change of the velocity of the molecules due to the rise of incoherent phenomena, which will be described in more details in the discussion of the results.

Flow instabilities studies

The velocity field $\mathbf{v}$ associated to the flow in a pipe could be considered[6] as the superposition of an average velocity $\mathbf{V}$ and a fluctuating part $\mathbf{u}$. Therefore, at a time t, the velocity $\mathbf{v}$ is defined by the relation

$$\mathbf{v}(t) = \mathbf{V} + \mathbf{u}(t) \tag{6}$$

Here $\mathbf{v}(t)$ denotes the time-dependent local velocity and the average $\mathbf{V}$ is given by:

$$\mathbf{V} = \lim_{t\to\infty} < \mathbf{v}(t) > \tag{7}$$

where the ensemble average $<\ldots>$ is taken over the distribution of velocity fields localized in space and the long-time limit is taken with respect to the longest correlation times of the velocity fluctuations.[9] The velocity fluctuations $\mathbf{u}(t)$ cause dispersion in the signal phase during acquisition, resulting in an image attenuation. This effect was visualized during imaging experiments resulting in an unexpected variation of the image features. A more detailed examination of the origin of such flow instabilities was performed by applying the NMR sequence based on the double PGSE method as described in the NMR experimental section (Figure 1c). The method is based on the evaluation of the different evolution of spins moving during the application of the two couple of pulsed field gradients able to encode translational information during the observation time Δ. The velocity data are then compared during the discussion to the well-known Reynolds number (Re), which indicates the ratio of inertial and viscous forces and is defined as:

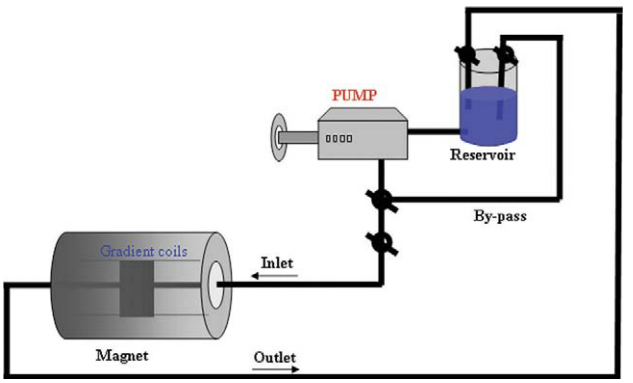

Figure 2. Scheme of the closed flow loop adapted to the NMR system, showing the pipe line running inside the superconducting magnet.

[Color figure can be viewed in the online issue, which is available at wileyonlinelibrary.com.]

$$Re = \frac{D \cdot \rho \cdot V}{\mu} \tag{8}$$

where D is the diameter of the pipe, ρ the density, μ is the dynamic viscosity of the fluid, and V the average velocity. In the case of time independent non-Newtonian fluids, the previous relation is no longer satisfied, as viscosity is known to decrease with the shear rate. In this case, a different parameter has to be used. We applied the generalized approach of Metzner and Reed,[10] which for a power-law fluid leads to a modified Reynolds number[11] defined by the following equation:

$$Re_{MR} = \frac{D^n V^{2-n} \cdot \rho}{8^{n-1} K \left(\frac{3n+1}{4n}\right)^n} \tag{9}$$

where K and n are constants, which can be experimentally determined.

Experimental

A closed flow loop[12] was realized (Figure 2) assembling polypropylene tubes in two configurations, reflecting different operative conditions: a single 13-mm internal diameter (I.D.) tube to simulate the fluid flow internally at a drilling string (Figure 3); two tubes of different diameter (13 and 30 mm I.D., respectively), one inside the other, with the smaller one rotating and adjustable in eccentric position, with the fluid flowing in the annular space between them. Such a configuration is to simulate the fluid flow in the wellbore, responsible for cutting transport to the surface (Figure 4). The position of the rotating rod inside the clear tube was regulated with micrometric mechanical control, while the rotating velocity was controlled by a hydro pneumatic motor. The pipes were joined by short flexible lines near the magnet entrance to allow easy access and removal. The NMR measurements were realized in the centre of the magnet by placing the coil around the straight line of the tube (Figure 3). The system was equipped with two screw-type pumps, which performed very stable flow conditions in the range of 5–120 cm s^{-1}, to mimic realistic flow rates in some portion of a drilling well. The pump flow rate was calibrated measuring the weight of the outcoming fluid at different time intervals

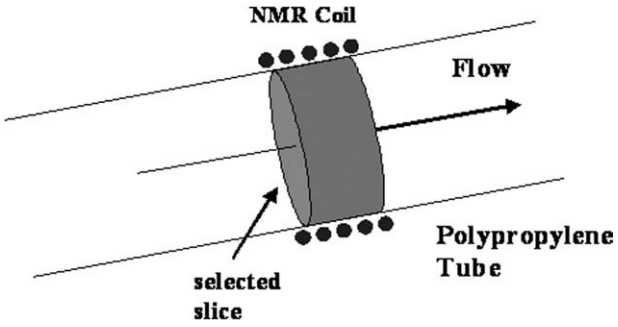

Figure 3. Scheme of the pipe section and the single slice excited in the MRI pulse sequence applied.

at several rates. To simulate drilling fluids, simplified polymer solutions were prepared by adding a pure grade Xanthan gum (Aldrich) to deionized water (0.3–0.5% w/w), adjusting at pH 10 with sodium hydroxide, and stirring overnight. The solution was then filtered and readily used. This polymer, at commercial grade, is used as a base in some drilling fluid formulations. The viscosity of the polymer solution was characterized by a commercial rheometer (RFS 3 by Rheometric Scientific) equipped with a micro-Couette geometry. The measurements were performed at 25°C, over a range of shear rates from 0.1 to 1000 s^{-1}. The typical shear-thinning behavior of the Xanthan solution is also shown by the rheological curve in Figure 5, where the plotted data show the decrease of viscosity vs. the shear rate. The Reynolds number corresponding to the different flow velocities of fluids were calculated according to Eq. 9 with $K = 1$ and $n = 0.33$ as experimentally found for the Xanthan solution at 0.3%. In the case of flow inside the annular system, a diameter D of 17 mm was used as input considering, as a first approximation, the clear section left as a circular tube itself.

Results and Discussion

Flow in the clear pipe

The NMR measurements with the PGSE imaging sequence as described in a previous paragraph were first applied to the study of the polymer solution flow (Xanthan gum in deionized water, 0.3% w/w) along a transverse slice (4-mm thick) in the pipe with I.D. 13 mm, as shown in Figure 3, perpendicular to the straight line. The flow measurements were performed keeping a steady-state flow at several

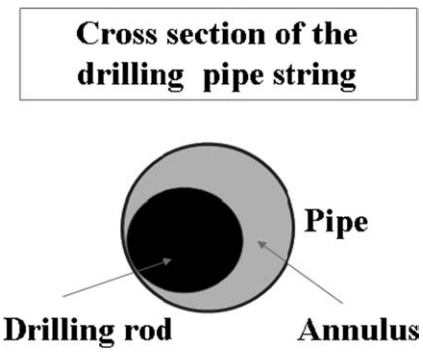

Figure 4. Scheme of the geometrical features adopted for the simulation of a well-drilling assembly.

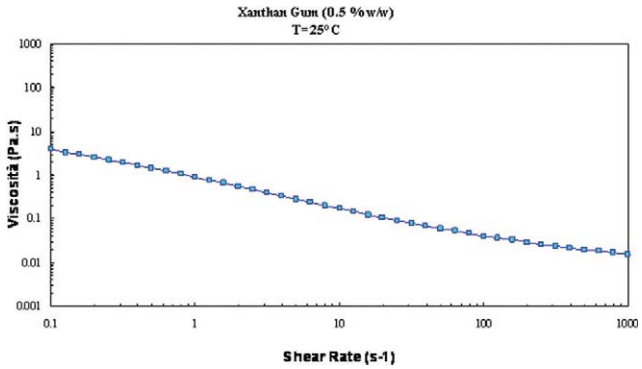

Figure 5. Rheogramme plotting dynamic viscosity vs. shear rate of the polymer (Xanthan Gum, 0.5% w/w) solution adopted in the flow experiments.

[Color figure can be viewed in the online issue, which is available at wileyonlinelibrary.com.]

average velocities, from 10 to 120 cm s^{-1}. The corresponding data are reported in Table 1, where the flow rate and the calculated velocity are compared with the NMR velocity measurements and the corresponding Reynolds number. In Figures 6a,b, the typical flow maps obtained by computing the velocities corresponding to a slice of the flowing fluid inside the pipe are reported. The NMR sequence allows measurements of the different phase shifts which are computed in the phase-sensitive images, associated to velocity values as already described in the previous sections. The two-dimensional (2D) velocity map obtained at the lowest pumping rate (run #1 in Table 1) is reported in Figure 6a, representing the velocity distribution along the pixel values in the image, whereas the corresponding three-dimensional (3D) plot (Figure 6b) gives an other representation of the data useful to visualize better the geometrical profile of the flow. From a statistical evaluation of the 2D map, an average velocity corresponding to 12.9 cm s^{-1} and a maximum velocity of 22 cm s^{-1} were calculated. The 3D plot (Figure 6b) shows a parabolic flow profile typically associated to a laminar regime as expected theoretically by the condition adopted. In such experimental conditions, because of the rather high viscosity and the rather low flow rate, the calculated Reynolds number, Re_{MR} (using the Metzner and Reed approach) is 41, to assess a typical laminar behavior. By increasing the flow rate (run #3 in Table 1) up to an average velocity of 27.9 cm s^{-1} (maximum velocity 51 cm s^{-1}), as computed statistically from the 2D map calculation (Re_{MR}=129), we still observe a macroscopic laminar regime (Figure 7a,b). The 1D velocity profiles obtained by plotting the data corresponding to the centre of the transverse section of the tube are shown in Figure 8. The best fit of these profiles was obtained by applying a power law model ($V = v_{max}\left[1 - \left(\frac{r}{R}\right)^{\frac{1}{n}+1}\right]$), where $n = 0.33$ was the best fitting parameter value. These results are in reasonable agreement with the expected viscoelastic behavior[11] of the polymers solutions applied in these experiments. A further increase of the flow rate (up to an average velocity of 58 cm s^{-1}) resulted in the prompt loss of the steady-state conditions, due the rise of flow instability effects. This behavior is

Table 1. List of Parameters Recorded on the Different Flow Experiments Performed on the Clear Tube (I.D. 13 mm) With the Xanthan Solution (0.3% w/w)

Run	Flow Rate ($cm^3\ s^{-1}$)	<v> (Volumetric, $cm\ s^{-1}$)	<v> (NMR, $cm\ s^{-1}$)	Flow Regime	Re_{MR}	Pump Regulator
#1	18.0	13.5	12.9	Laminar	41	2
#2	29.3	22.0	21.5	Laminar	83	4
#3	37.4	28.1	27.9	Laminar	129	5
#4	47.7	35.8	35.8	Laminar	141	6
#5	60.8	45.7	42.9	Laminar	264	7
#6	77.6	58.4	–	Turbulent	440	8
#7	126.0	95.0	–	Turbulent	990	10

The average flow velocities are determined volumetrically and from velocity encoding NMR.

confirmed by the lose of phase coherence in the NMR transverse magnetization, characterized by a significant signal loss due to the typical unsteady-state condition associated to a turbulent regime, as specifically described in the following paragraphs. This early transition (characterized by a calculated $Re_{MR} = 440$) from laminar to turbulent flow pattern is far behind the theoretical value of $Re = 2300$, which should be reasonably expected for the change of transport regime in Newtonian fluids.[11] As complex flows of some viscoelastic fluids are believed to develop instabilities or turbulence[13] at very low flow rates that are usually absent in the flow of pure Newtonian fluids, we further tried to investigate this particular behavior by applying another suitable method based on different measurements, as will be described in a dedicated paragraph.

Flow instabilities in laminar regime

This early transition from laminar to turbulent regime could be investigated experimentally by measuring directly

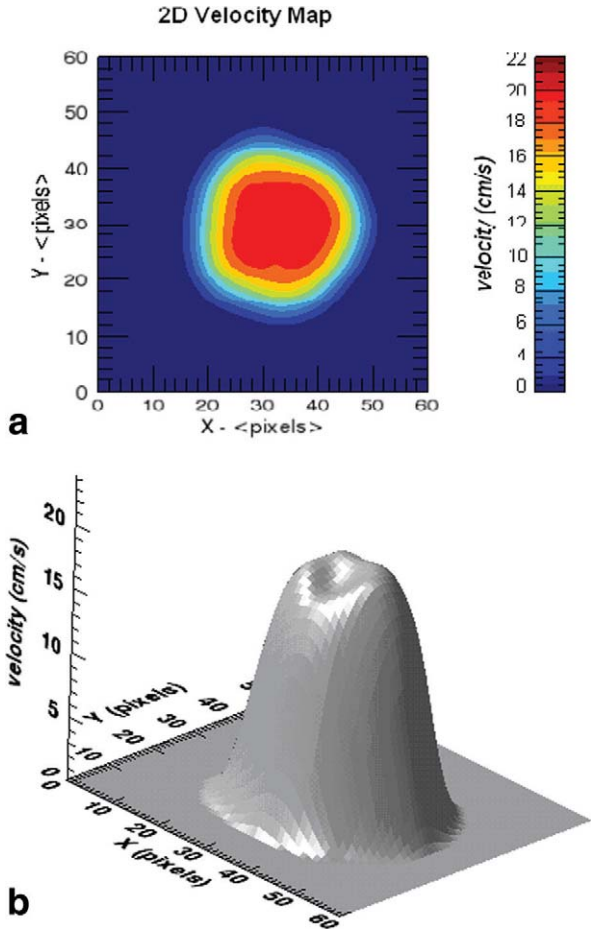

Figure 6. 2D velocity map (a) of the Xanthan solution (0.3% w/w) flowing in the 13-mm pipe (run #1 in Table 1) and the corresponding stacked plot (b) to emphasize the 3D spatial distribution.

[Color figure can be viewed in the online issue, which is available at wileyonlinelibrary.com.]

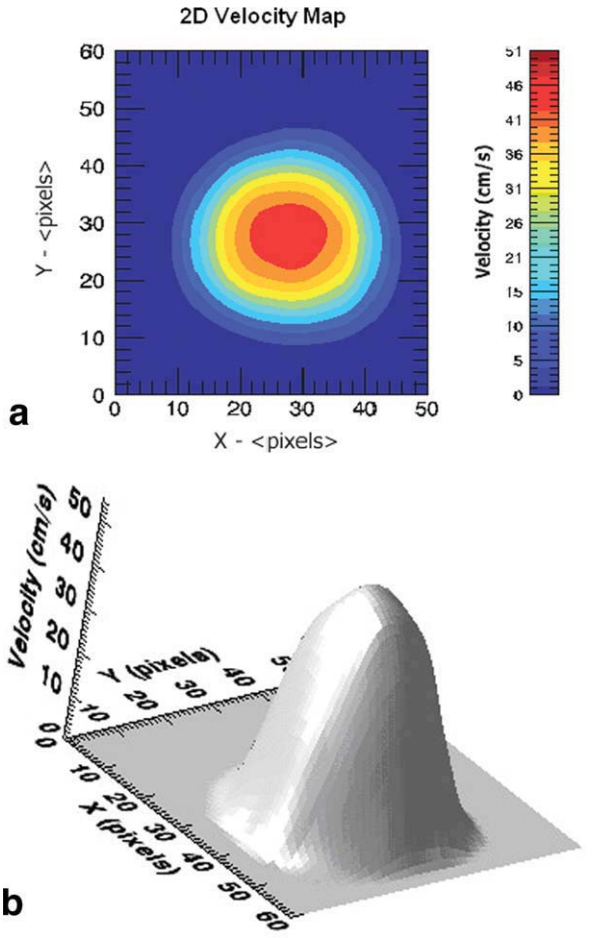

Figure 7. 2D velocity map (a) for the Xanthan solution (0.3% w/w) flowing in the 13-mm pipe (run #3 in Table 1) and the corresponding stacked plot (b) to emphasize the 3D spatial distribution.

[Color figure can be viewed in the online issue, which is available at wileyonlinelibrary.com.]

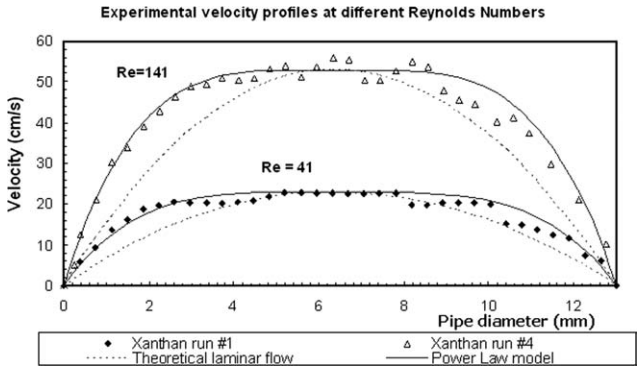

Figure 8. Maximum velocity profiles measured on the middle of the clear tube of the flow of the Xanthan Gum (0.3%) solution inside the assembled 13-mm pipe.

By applying the power law model ($V = v_{\max}\left[1 - \left(\frac{r}{R}\right)^{\frac{1}{n}+1}\right]$), a value of $n = 0.33$ was found.

the rise of velocity fluctuations. A part of our work was directed to assess this particular subject, with the aim to analyze it directly by suitable experiments. The double PGSE NMR sequence, described in a previous paragraph, was applied on the experiments performed on the clear 13-mm tube to analyze the already observed changes in the flow regime. The measurements were performed by acquiring the NMR signal at different flow rates, starting from low (47.7 $cm^3\ s^{-1}$ with $Re_{MR} = 141$) to high values 77.6 $cm^3\ s^{-1}$ with $Re_{MR} = 440$ and 126 $cm^3\ s^{-1}$ with $Re = 990$) in a range of expected turbulence. The effect of this sequence is causing a phase shift related to fluctuations in the motion over the evolution (or exchange) time τ_m between the pulsed gradients pairs. In Figure 9, the averaged functions of the spins displacements ($\tau_m = 20$ ms) are plotted vs. the velocity variation. The results obtained are compared, and the plots clearly show an increase of the width of the function (P_v) of the

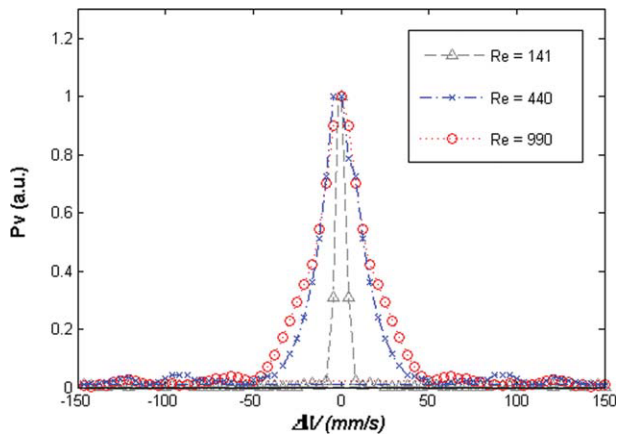

Figure 9. Averaged probability of velocity (P_v) resulting from a compensated double PGSE experiment (VEXSY-1D) on a flowing solution of Xanthan Gum (0.3% w/w) at different flow rates (refer to Table 1: *Re* = 141, 441, and 990).

[Color figure can be viewed in the online issue, which is available at wileyonlinelibrary.com.]

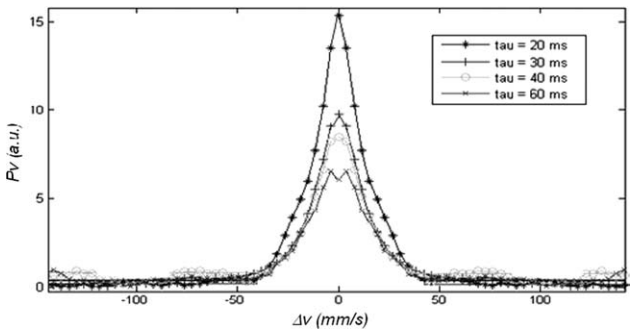

Figure 10. Averaged probability of velocity (P_v) resulting from a compensated double PGSE experiment (VEXSY-1D) on a flowing solution of Xanthan Gum (0.3% w/w) at different tau (exchange time τ_m).

variation of velocity ΔV with the increase of the flow rate, indicating a larger spreading of the velocity variation of the spins ensemble during the observation time. The incidence of velocity changes is limited at the low flow rate ($Re_{MR} = 141$), where the pure diffusive flow is dominant, while the effect becomes very significant when the flow approaches the turbulent regime (*Re* from 440) with a strong spreading of the velocity change function. This experimental observation is a quantitative indication of the velocity fluctuations rising with the flow rate, clearly correlated to the occurring flow instabilities. Moreover, as shown in Figure 10, a plot of the several measurements taken at the highest flow rate ($Re_{MR} = 990$) at increasing values of the evolution time from 20 to 60 ms, show a dependence on τ_m, which is related with the time scale of the occurring dynamic phenomena. The velocity instabilities are due to the velocity variation or acceleration of the flowing molecules during the translation, probably related to the dynamic properties induced by the polymer molecules. The ensemble of the molecules' velocity fluctuations is the cause of the macroscopically observed early transition to a disordered flow regime. According to Groisman and Steinberg,[14,15] the rise of marked flow instability at low *Re*, called "elastic turbulence" (in contrast to the usual inertial turbulence, which is observed in Newtonian fluids at high *Re*), is a consequence of the stretching of polymer chains.

Flow in the annular geometry

The considerations based on the experimental section reported in the previous paragraphs are valid for flow in a clear pipe. However, most of the industrial applications involving polymer fluids are designed for complex plants with considerable geometrical constrictions. In the attempt of simulating the case of drilling operational technology, we built a special pipe with a rotating drilling rod inside, as schematically reported in the experimental part (Figure 4). This special section was added to the flow loop already described with the specific aim to simulate the effect of different fluids and applied conditions on flow behavior. In such a case, the pipe diameter was increased to 30 mm to accommodate the rod inside. The position of the rotating rod was regulated with micrometric mechanical control, to get a

Table 2. List of Parameters Recorded on the Different Flow Experiments Performed on the Assembled Tube (I.D. 30 mm) With the Xanthan Solution (0.5% w/w)

Run	Flow Rate ($cm^3\ s^{-1}$)	<v> (Volumetric, $cm\ s^{-1}$)	$<v>_{NMR}$ (NMR, $cm\ s^{-1}$)	Flow Regime	Re_{MR}	Pump Regulator
#8	60	8.9	9.5	Laminar	23	1.4
#9	213	31.5	31.4	Laminar	172	1.6
#10	339	50.4	55.0	Laminar	438	1.8
#11	500	74.1	–	Turbulent	719	2.0
#12	694	102.8	–	Turbulent	1243	2.5

The average flow velocities are determined volumetrically and from velocity encoding NMR.

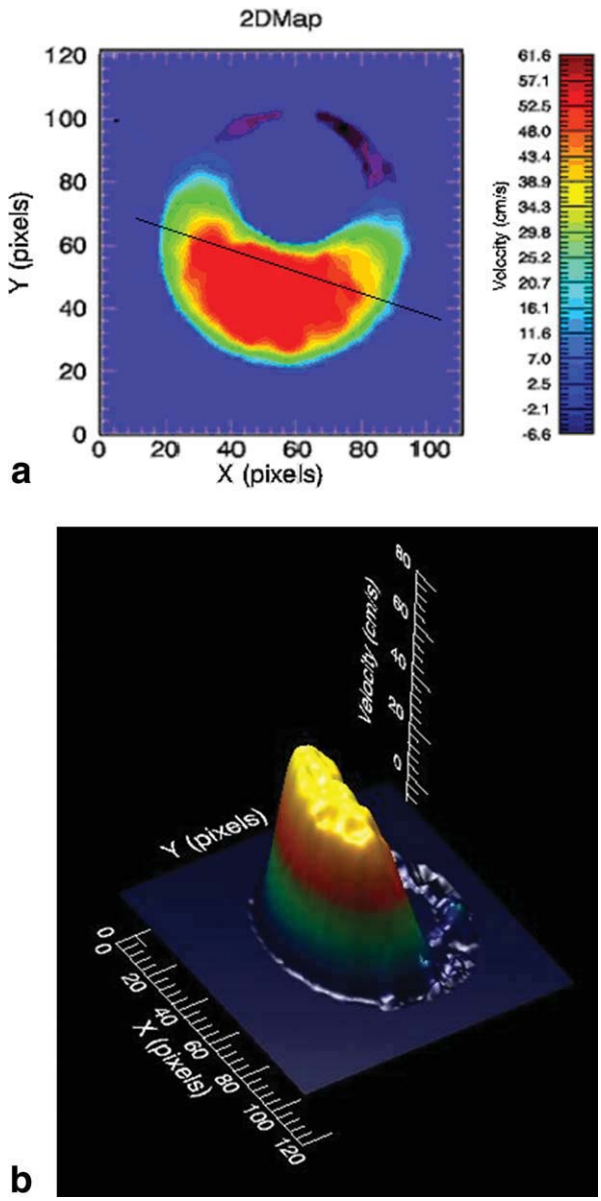

Figure 11. 2D velocity map (a) of the Xanthan Gum (0.5% w/w) solution flowing in the 30 mm pipe (run #9 in Table 2) and the corresponding stacked plot (b) to emphasize the 3D spatial distribution.

[Color figure can be viewed in the online issue, which is available at wileyonlinelibrary.com.]

slight eccentricity. Flow modifications, due to geometrical restriction,[16] were observed by examining the velocity maps obtained by MRI. One of the most representative 2D flow maps (run #9 described in Table 2) is shown in Figure 11a, whereas the corresponding three-dimensional plot (Figure 11b) gives an aid to the visualization of the geometrical profile. The 2D flow map shows a clearly heterogeneous distribution of the flow velocity in the transversal section examined, with rather absence of fluid passage on the top of the image where the restriction is more pronounced. The highest flow velocities are clearly located in the centre of the flow line where the clearance is maxima, confirming the laminar regime conditions. By analyzing this region, an average velocity of 31.4 $cm\ s^{-1}$ was calculated corresponding to $Re_{MR} = 172$. The flow map also shows a region where the velocity goes to zero before presenting a slight counterflow and higher where the clearance is minimal. This phenomenon appears when the internal rod eccentricity is high (close to the external pipe) and is more pronounced at high flow rates (not reported here). It seems not to be generated by either pipe restrictions in the flow loop (carefully avoided) or spurious signals in the background (nothing similar was detected in the experiments performed in the single pipe). The origin of this phenomenon is unknown. A typical velocity profile obtained by plotting the data corresponding to the central region of the tube (see the line in Figure 11), where the velocity was reasonably not influenced by geometrical constrictions is reported in Figure 12. Despite to the different geometry, the profile is apparently in agreement with the model fitting applied on the clear 13 mm tube, as reported in the previous paragraph. Increasing the flow rate to 339 $cm^3\ s^{-1}$,

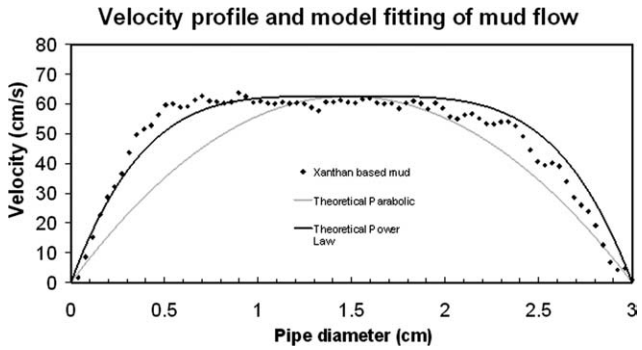

Figure 12. Maximum velocity profile measured on the middle of the annular section of the tube (Figure 9) of the flow of the Xanthan Gum (0.5 %) solution inside the assembled 30-mm pipe.

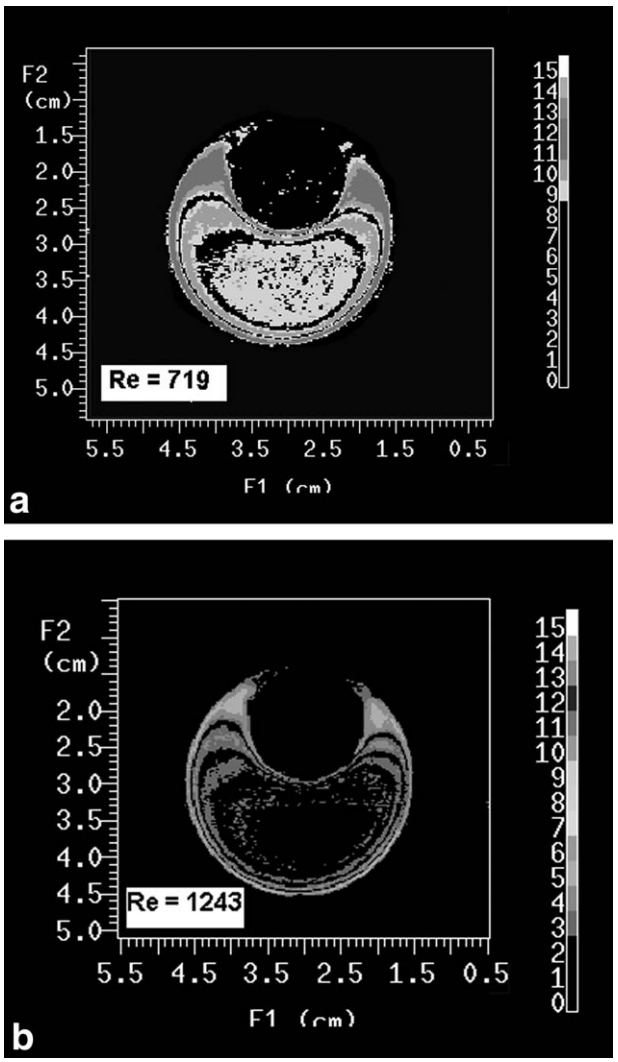

Figure 13. Flow velocity weighted images of the Xanthan Gum (0.5% w/w) solution flowing in the 30-mm tube at different rates (runs #10 and #11 in Table 1), corresponding to *Re* = 719 (a), 1243 (b).

corresponding to an average velocity of 50.4 cm s^{-1} (Re_{MR} = 438), a laminar regime is still observed (run #10). Deviations from laminar conditions, as reported in Table 2, could be appreciated (Figure 13) from the flow-weighted images, which are sensitive to flow velocity changes (velocity maps are not obtainable because of the severe distortions). These flow experiments (runs #11 and #12) were performed at higher fluid average velocity (74.1 cm s^{-1}, Figure 13a, and 102.8 cm s^{-1}, Figure 13b) and the images show an increasing attenuation of the signal in the central region due to the loss of signal phase coherence determined by the rise of the velocity fluctuations.

The presence of low velocity or stagnant flow areas and the rise of turbulent flow could negatively influence the transport and removal of solid particles related to the drilling operations. The stagnation and reflux of rock ablating particles could create severe problems in clearing the wellbore and resulting in obstructions or tools damage.

Conclusions

MRI methods have a great potential in providing valuable data as an aid to simulation of complex engineering operations in which flow dynamics is involved. The flow regime involved in the dynamic of polymer solutions is especially complex even at very low flow rates. In fact, an early transition from laminar to turbulent flow regime was observed at very low Reynolds number. This effect was demonstrated on these materials by using an NMR imaging method that was able to directly observe velocity variation in the system avoiding any interference. This effect is likely determined by the elastic properties of the polymer chains,[14,15,17–19] which induce mechanical perturbation under stress. Rheological properties and restrictions or geometrical features introduced in the flow line to simulate pipe lines and drilling tools consistently modified the flow dynamics, giving rise to velocity variation and fluctuations. This observation confirmed the theoretical considerations and typical rheological measurements performed on similar molecules. The experimental measurement of flow parameters by imaging techniques could be very useful in providing experimental data to assess numerical simulations of complex engineering processes such as the drilling operations.

Acknowledgments

The authors thank the management of Eni E&P and R&M divisions for funding and permission to publish this work. Mr. A. Efori and Mr. A. Omini are also gratefully acknowledged for their help in the experimental activity. They thank Mr. Peveri, from WEI International, for the flow loop realization.

Notation

$\mathbf{G}$ = magnetic field gradient, Gauss m^{-1}
$\mathbf{V}$ = average fluid velocity, m s^{-1}
$\mathbf{Z}$ = displacement along direction of flow, m
D = pipe diameter, m
R = pipe radius, m
E = echo amplitude of NMR signal, arbitrary units
P = distribution function of molecular displacements
TE = echo time, s
TR = recovery time, s
K = power law consistency index, kg m^{-1} s^{2-n}
$\boldsymbol{q}$ = reciprocal space, $[=(2\pi)^{-1}\gamma\mathbf{G}\delta]$, m^{-1}
r = radius ($r \leq R$), m
z = direction along the flow, m
t = time, s
$\mathbf{v}$ = local fluid velocity, m s^{-1}
$\mathbf{u}$ = fluctuating part of velocity, m s^{-1}
$\boldsymbol{g}$ = gradient constant, T m^{-1}

Greek letters

τ_m = exchange time or mixing time, s
Δ = time interval, s
γ = gyromagnetic ratio
μ = dynamic viscosity, Pa s
ρ = density of fluids, Kg m^{-3}
ϕ = phase shift, rad
δ = flow encoding gradient duration, s

Dimensionless quantities

Re = Reynolds number, $[= D \cdot \rho \cdot V/\mu]$
Re_{MR} = Generalized Reynolds number, $[= D^n V^{2-n} \cdot \rho/8^{n-1} K (3n + 1/4n)^n]$
n = power law index

Subscripts

z = coordinate along flow direction
v = velocity encoding

Literature Cited

1. Stapf S, Song-I Han, editors. *NMR Imaging in Chemical Engineering*. Weinheim, Germany: Wiley-VCH, 2006.
2. Callaghan PT. *Principles of NMR Microscopy*. Oxford: Oxford University Press, 1991.
3. Callaghan PT, Eccles CD, Xia YJ. NMR microscopy of dynamic displacement. *J Phys E: Sci Instrum.* 1988;21:820–822.
4. Blumich B. *NMR Imaging of Materials*. Oxford: Oxford University Press, 2000.
5. Irwin NC, Greenkorn RA, Altobelli SA, Cusham JH. Examination of transport theory of arbitrary order in velocity variance by MRI. *AIChE J*. 1999;45:1351–1354.
6. Callaghan PT, Codd SL, Seymour JD. Spatial coherence phenomena arising from translational spin motion in gradient spin echo experiments. *Concepts Magn Reson.* 1999;14:181–202.
7. Han S, Stapf S, Blumich B. Two dimensional PFG NMR for encoding correlations of positions, velocity and acceleration in fluid transport. *J Magn Reson.* 2000;146:169–180.
8. Callaghan PT, Khrapitchev AA. Time dependent velocities in porous media dispersive flow. *Magn Reson Imaging*. 2001;19:301–305.
9. Koch DL, Brady JF. The effect of order on dispersion in porous media. *J Fluid Mech.* 1989;200:173.
10. Metzner AB, Reed JC. Flow of non Newtonian-fluids correlation of the laminar, transition and turbulent flow regions. *AIChE J*. 1955;14:434–440.
11. Perry RH, Green DW. *Perry's Chemical Engineers' Handbook*, *8th ed*. New York: McGraw-Hill, 2007.
12. Donaggio F, Mancini N, Maddinelli G, Correra S. Fluent CFD code performance evaluation in describing oil in water dispersions flow. *Proc 3rd Int Conf Multiphase Flow*. Pisa: Italy, April 1999.
13. Cruz DO, Pinho FT. Turbulent pipe flow predictions with low Reynolds number for drag reducing fluids. *J Non-Newtonian Fluid Mech.* 2003;114:109–148.
14. Groisman A, Steinberg V. Elastic turbulence in a polymer solution flow. *Nature*. 2000;409:53–55.
15. Groisman A, Steinberg V. Stretching of polymers in a random three-dimensional flow. *Phys Rev Lett*. 2001;86:934–937.
16. Xia Y, Callaghan PT, Jeffrey KR. Imaging velocity profiles: flow through an abrupt contraction and expansion. *AIChE J*. 1992;38:1408–1420.
17. Liberzon A, Guala B, Lotni B, Kinzelbach W, Tsinober A. Turbulence in dilute polymer solutions. *Phys Fluids*. 2005;17:031707.
18. Fouxon A, Lebedev V. Spectra of turbulence in dilute polymer solutions. *Phys Fluids*. 2003;15:2060–2072.
19. Lumley JL. Drag reduction in turbulent flow by polymer additives. *J Polym Sci: Macromol Rev*. 2003;7:263–290.

Manuscript received Nov. 4, 2009, revision received Apr. 13, 2010, and final revision received Jun. 22, 2010.